Ground Support 2026 - D Cumming-Potvin & J Wesseloo (eds.)
© 2026 Australian Centre for Geomechanics, Perth
doi:10.36487/ACG_repo/2625_21

An artificial-intelligence-enhanced approach for ground stability assessment using large-scale datasets of rockbolt load and roadway convergence

Fuqiang Gao [a,b,*], Hongpu Kang [a,b], Wenju Liu [a,b]

[a] *Coal Mining Research Institute, China Coal Technology and Engineering Group, China*

[b] *State Key Laboratory of Intelligent Coal Mining and Strata Control, China Coal Research Institute, China*

Abstract

Ground stability assessment is a fundamental requirement for maintaining the safety and functionality of underground openings such as coal mine roadways and tunnels. Conventional assessment methods often rely on sparse measurements and manual interpretation, which limit both accuracy and efficiency. To overcome these limitations, we propose a novel data-driven approach that integrates LiDAR-based 3D scanning with deep learning algorithms to automatically identify rockbolts, measure bolt loads, and measure roadway convergence with high precision. By combining these 2 extensive datasets, we establish a comprehensive framework for evaluating ground stability and detecting zones susceptible to instability or rockfall. The developed method enables continuous, automated monitoring and significantly improves the reliability of stability evaluation compared with traditional visual or point-based measurements.

Keywords: *roadway, rockbolts, laser scanning, artificial intelligence*

1 Introduction

Ground support is essential for maintaining the stability and serviceability of underground excavations, particularly in coal mine roadways where deformation, roof separation and local rockfalls may develop under complex geological and mining-induced conditions (Kang et al. 2023). Rockbolts and cable bolts are the most widely used reinforcement elements, but their actual performance is rarely assessed at roadway scale. Conventional monitoring typically relies on a small number of extensometers, convergence stations or instrumented bolts. These measurements provide accurate local information, but they are spatially sparse and may not represent the overall behaviour of the supported roadway. As a result, the interaction between surrounding rock deformation and support loading is often interpreted from incomplete evidence. In recent years, 3D laser scanning has been increasingly used for repeated or semi-continuous monitoring of excavation deformation, providing high-density measurements over large areas. However, while considerable effort has been devoted to extracting roadway deformation from these datasets, the use of the same scanning data to determine the loads carried by rockbolts has received little attention.

To address this limitation, a non-destructive method was previously developed to estimate the axial load of a rockbolt from the deformation of its bearing plate (Liu et al. 2024). The method uses 3D laser scanning to capture the bearing-plate geometry and a convolutional neural network to establish the relationship between plate deformation and bolt load. Laboratory validation showed that bolt axial loads could be estimated with an average error of approximately ±15 kN. More recently, an enhanced PointNet++ segmentation framework combined with a normalisation preprocessing head and a coverage-voted strategy was developed to automatically identify bearing plates, metal mesh and surrounding rock from large

* Corresponding author. Email address: fuqgao@gmail.com

roadway point-cloud datasets (Liu et al. 2026). The method achieved an overall segmentation accuracy of about 94%, enabling multiple rockbolts to be identified and assessed from a single scan.

The present study extends these developments from method validation to field-scale ground stability assessment. A coal mine roadway was scanned to obtain 2 complementary large-scale datasets: the axial loads of multiple rockbolts and the deformation field of the surrounding rock mass. These datasets provide different but closely related information. Roadway convergence reflects the geometric response of the rock mass, whereas bolt load reveals the mobilisation and spatial distribution of support resistance. Their combined interpretation makes it possible to distinguish zones of low deformation and low support demand from areas characterised by concentrated bolt loading, excessive convergence or an abnormal mismatch between deformation and support response.

This paper presents the integrated measurement workflow and its field implementation. The proposed approach offers a practical basis for identifying potentially unstable zones and for developing more reliable, data-supported ground control decisions.

2 The novel method for measuring rockbolt loads and roadway deformation

The proposed method uses a single 3D laser-scanning dataset to obtain both the deformation of the roadway surface and the loads carried by multiple rockbolts. The overall workflow consists of point-cloud acquisition, automatic identification of support components, bolt-load estimation and multi-epoch deformation calculation, as shown in Figure 1.

2.1 Point-cloud acquisition and support-component identification

The roadway was scanned using a stationary Z+F IMAGER 5016A terrestrial laser scanner, with a ranging error of approximately ±1 mm, allowing the generation of a dense 3D point cloud containing the surrounding rock surface, bearing plates, cable plates and steel mesh. Because a roadway scan may contain millions of points and support components occur at different spatial scales, the original point cloud is divided into overlapping local grids before segmentation.

An enhanced PointNet++ model is then used to classify each point as surrounding rock, bearing plate or steel mesh, see Figure 2. A normalisation preprocessing head based on principal component analysis is introduced to reduce the influence of grid orientation. In addition, 4 overlapping grid systems are applied so that each support component is completely covered in at least one grid. The segmentation results from the 4 grids are combined through a voting strategy. In the previous field validation, this method achieved an overall segmentation accuracy of approximately 94%, while the intersection-over-union value for bearing plates reached 0.78.

The segmented bearing plates are subsequently extracted from the roadway point cloud, allowing the spatial coordinates and geometric characteristics of individual rockbolts and cable bolts to be determined automatically.

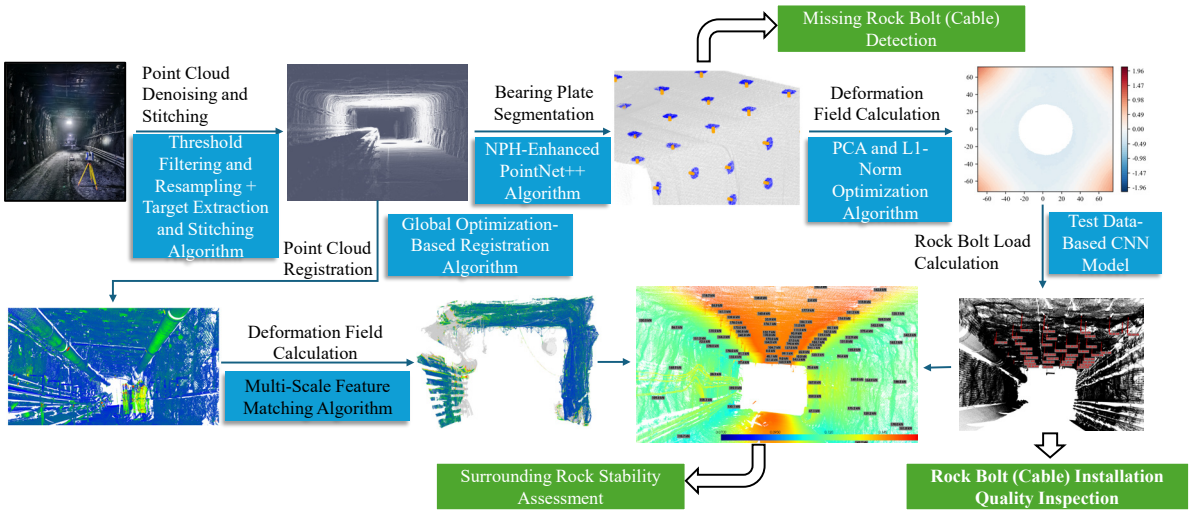


Figure 1 Overall workflow for simultaneous measurement of roadway deformation and rockbolt loads using 3D laser scanning and deep learning

2.2 Measurement of rockbolt axial load

The axial load of each rockbolt is estimated from the deformation pattern of its bearing plate. As bolt load increases, the plate bends against the roadway surface, producing a 3D deformation field related to the applied axial force. The plate point cloud is aligned and normalised using iterative closest point registration, principal component analysis and an L1-norm minimisation procedure. The signed distance between the loaded plate surface and its reference geometry is then calculated to generate a standardised deformation field.

A convolutional neural network, termed the rockbolt force testing model, is used to map the plate deformation field to bolt axial load. The model was trained and validated using laboratory pull-out tests covering different load levels and installation angles. The reported mean absolute prediction error was approximately 5 kN, demonstrating that plate deformation can be used as a non-destructive indicator of bolt load. It should be noted that the load-estimation model is specific to the bearing-plate configuration used for training. If bearing plates with substantially different materials, dimensions, shapes, or profiles are used, pull-out tests are required to establish a new bolt load–plate deformation dataset and retrain the model accordingly.

By combining automatic bearing-plate segmentation with the trained load-estimation model, the axial loads of many bolts can be obtained from one roadway scan rather than by installing sensors on selected bolts.

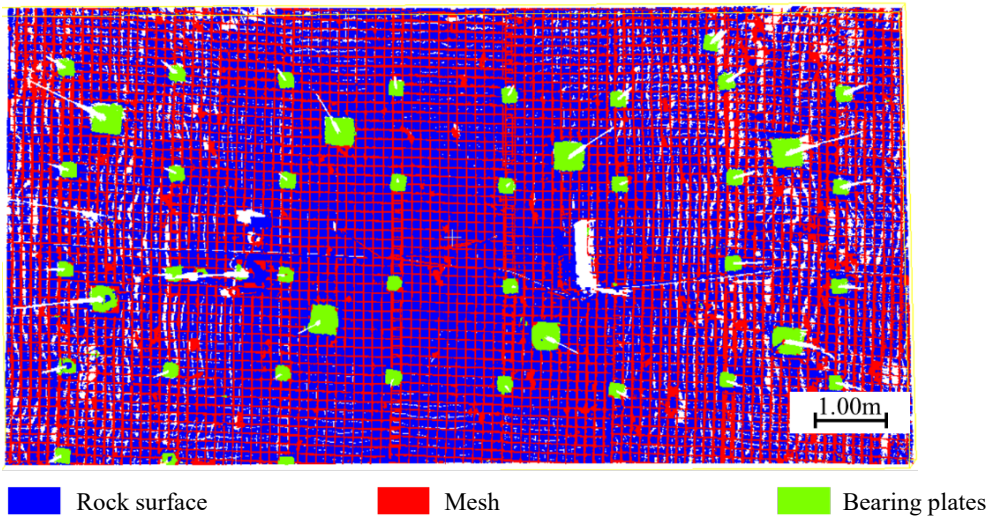


Figure 2 Automatic segmentation of roadway support components from the 3D point cloud

2.3 Measurement of roadway deformation

Roadway deformation is determined by comparing point clouds collected at different monitoring times. After removal of temporary objects and support components where necessary, the multi-epoch point clouds are registered within a common coordinate system. The signed distance between corresponding roadway surfaces is then calculated to obtain the full-field displacement distribution.

The resulting deformation dataset describes roof sag, rib convergence, floor heave and local surface deformation along the monitored roadway. It should be noted that floor displacement requires particular caution because roadway cleaning, grading and other operational activities may alter the floor surface between successive scans. Such changes should be excluded from the deformation analysis where identifiable, and floor deformation should only be interpreted when persistent or clear heave features are observed. Bolt-load data and roadway deformation data are referenced to the same spatial coordinate system, enabling the mechanical response of the support system to be directly compared with the surrounding rock response. This integrated dataset forms the basis for the roadway stability assessment presented in the following section.

3 Field application

3.1 Site and engineering conditions

Field testing was conducted in the No. 3305 return-air roadway of the Tiandi Wangpo Coal Mine, located in Zezhou County, Jincheng City, Shanxi Province, near the southeastern margin of the Qinshui Coalfield. The mine has a designed production capacity of 3.0 Mt/a. The geological structure of the mining area is relatively complex and is mainly controlled by the Neocathaysian structural system.

The principal mineable seam is the No. 3 coal seam, with an average thickness of 5.27 m and a uniaxial compressive strength (UCS) of 15 MPa. Joints and fractures are highly developed within the coal and surrounding strata. From top to bottom, the immediate geological sequence comprises an 8.89 m-thick medium sandstone main roof with a UCS of 74.1 MPa; a 4.00 m-thick sandy mudstone immediate roof, locally containing coarse siltstone, with a UCS of 41.6 MPa; and a 0.30 m-thick carbonaceous mudstone false roof with a UCS of 11.0 MPa. The immediate floor consists of mudstone or fine siltstone, with an average thickness of 2.10 m and a UCS of 36.7 MPa, while the main floor is medium sandstone, averaging 3.20 m in thickness and 74.1 MPa in UCS.

The mine adopts a panel-based development layout. Longwall faces are generally 150–200 m wide and advance at approximately 3–5 m/d. The development roadways are rectangular coal roadways excavated along the floor while retaining a layer of top coal. The tested roadway has a rectangular cross-section with a width of 5.0 m and a height of 3.6 m, corresponding to an area of 15–18 m².

Ground support consists of a combined rockbolt–cable bolt system. The rockbolts are 2.4 m long and installed at spacings and row spacings of approximately 0.8–1.0 m. The rockbolts are 22 mm in diameter, with a capacity of 255 kN and are partially bonded. The cable bolts are 7.3 m long and arranged in a 3–0–3 pattern, with a spacing of 1.5 m and a row spacing of 2.0 m. The cable bolts are 21.8 mm in diameter, with a capacity of 582 kN, and are also partially bonded. Welded steel meshes are installed on the roof, whereas chain-link meshes are used on the ribs.

The roadway is influenced by collapse columns, faults and folds. In some sections, the coal and surrounding rock are extremely weak and fractured, and severe roof falls occasionally occur during roadway development. After exposure to mining-induced stress, localised roof sag, rib bulging and floor heave have also been observed. These complex geological and deformation conditions provide a suitable environment for evaluating the field performance of the proposed measurement system. The No. 3305 return-air roadway was therefore selected for the field application.

3.2 Field measurement procedure

Laser scans were conducted at selected sections of the roadway using a terrestrial 3D laser scanner (Figure 3). The scanning locations and ranges were arranged to capture the roadway surface, steel mesh and bearing plates of the installed bolts. The acquired point clouds were processed using the enhanced segmentation algorithm described in Section 2 to identify the roadway surface and individual bearing plates.

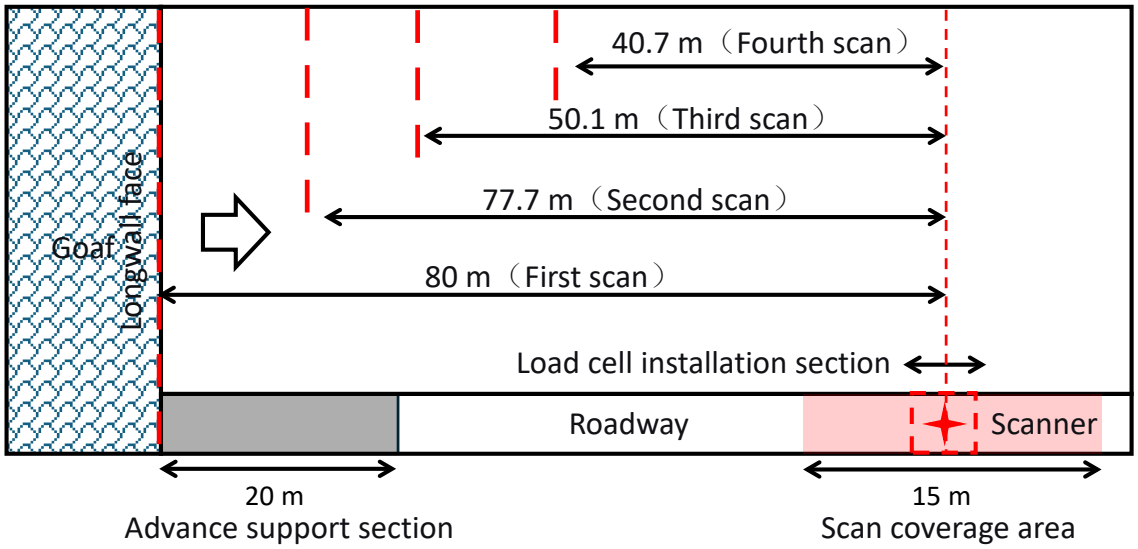


Figure 3 Location of the scanning section

The segmented bearing-plate point clouds were subsequently analysed using the trained bolt-load estimation model to determine the axial load of each identified bolt. Repeated scans of the same roadway section were registered in a common coordinate system, and the surface-to-surface distances between different scanning epochs were calculated to obtain the roadway deformation field. The bolt-load and deformation results were finally mapped onto the same roadway coordinate system, enabling direct comparison between support loading and surrounding-rock response.

3.3 Evolution of roadway deformation and rockbolt loading

Figures 4 and 5 show the measured evolution of the roadway deformation field and rockbolt loads as the longwall face approached the monitored section. At a face distance of 77.7 m, the roadway response was relatively limited and spatially uniform. Most of the monitored surface remained close to the reference condition, indicating that mining-induced disturbance at this stage was weak. The corresponding bolt-load distribution was also relatively dispersed, with no pronounced concentration of highly loaded bolts.

When the face advanced to 50.1 m from the monitored section, the roadway deformation increased noticeably. The deformation field became more heterogeneous, with distinct localised zones developing along the roof and ribs. The internal view of the roadway further shows that the deformation was not uniformly distributed around the perimeter; instead, several concentrated deformation bands were present, reflecting the combined effects of roadway geometry, local geological weakness and the approaching mining-induced stress field. At the same time, the load carried by the rockbolt system became more spatially differentiated, suggesting that the support load was being redistributed from relatively uniform mobilisation to a more concentrated pattern.

At a face distance of 40.7 m, both the magnitude and spatial extent of roadway deformation increased further. The roof and upper ribs exhibited the most evident changes, while local zones of concentrated deformation expanded along the roadway. The bolt-load results show a corresponding increase in the number and spatial clustering of mobilised bolts. This indicates that the support system progressively responded to the mining-induced deformation, with some bolt groups carrying a greater proportion of the redistributed load.

The combined results demonstrate that roadway deformation and bolt loading evolved in a closely related but spatially non-uniform manner. Zones with greater deformation generally coincided with areas where bolt loads became more concentrated, indicating stronger mobilisation of the support system. However, the correspondence was not perfectly uniform along the roadway, which highlights the limitation of relying on a small number of instrumented bolts or convergence points. A locally installed sensor could either miss a highly affected zone or overrepresent an isolated response. In contrast, the proposed method provides roadway-scale distributions of both deformation and support loading, allowing the progression of mining-induced ground response to be assessed more comprehensively.

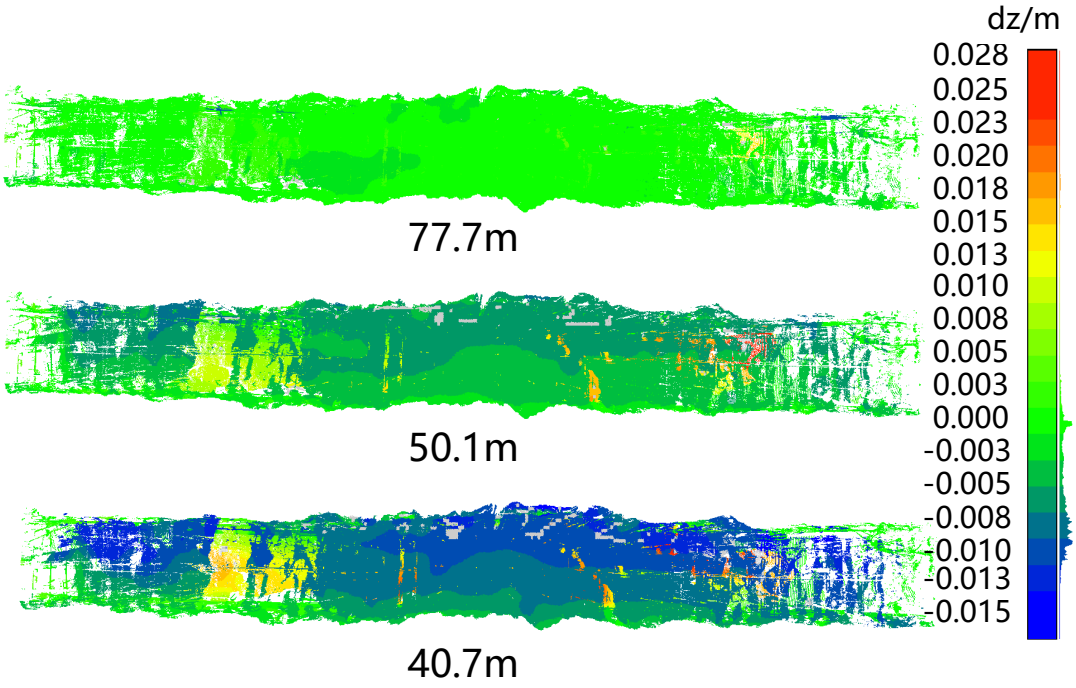


Figure 4 Evolution of the deformation field of a section of roadway as longwall face approaches. The data below each figure indicates the distance of the longwall face

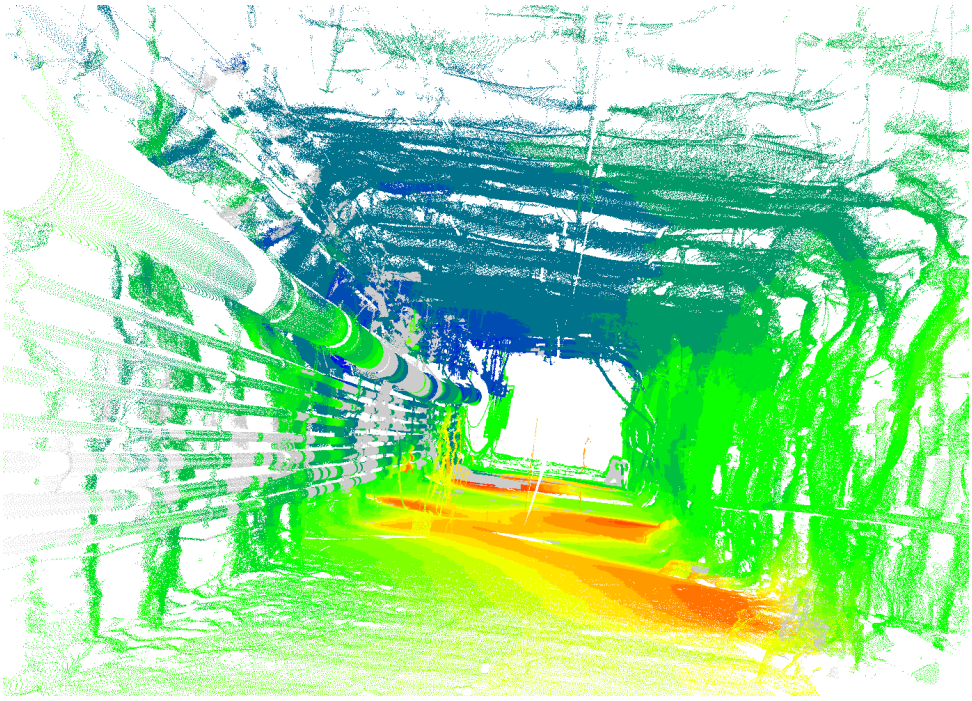


Figure 5 Deformation field of the roadway from a view inside the roadway. The scale is the same as Figure 3

4 Conclusion

A field-scale method was developed to jointly measure roadway deformation and the axial loads of multiple rockbolts using terrestrial laser scanning and deep learning. Automatic point-cloud segmentation enables bearing plates and surrounding rock surfaces to be extracted from a single scan, while the bearing-plate deformation model provides non-destructive estimation of bolt loads. Application in the No. 3305 return-air roadway demonstrated that the method can capture the spatially non-uniform evolution of both roadway convergence and bolt-load redistribution as the longwall face approaches. The results showed increasing deformation localisation and progressive mobilisation of the support system under mining-induced disturbance. Compared with conventional point-based monitoring, the proposed approach provides a more representative description of the roadway–support response and offers a practical basis for identifying locally disturbed zones and assessing ground stability at roadway scale.

Acknowledgement

This work has been supported by the National Natural Science Foundation of China (grant No. 52325403).

References

Kang, H, Gao, F, Xu, G & Ren, H 2023, 'Mechanical behaviors of coal measures and ground control technologies for China's deep coal mines – A review', *Journal of Rock Mechanics and Geotechnical Engineering*, vol. 15, no. 1, pp. 37–65, https://doi.org/10.1016/j.jrmge.2022.11.004

Liu, W, Gao, F, Dong, S & Yuan, G 2024, 'A novel method for estimating axial force of rock bolt through 3D laser scanning and deep learning', *Rock Mechanics and Rock Engineering*, vol. 57, no. 2, pp. 1437–1450, https://doi.org/10.1007/s00603-023-03638-z

Liu, W, Gao, F, Dong, S, Wang, X, Cao, S, Wang, W & Liu, X 2026, 'An enhanced segmentation method for 3D point cloud of tunnel support system using PointNet++ and coverage-voted strategy algorithms', *Journal of Rock Mechanics and Geotechnical Engineering*, vol. 18, no. 2, pp. 1653–1660, https://doi.org/10.1016/j.jrmge.2025.03.039